Monthly Notices
of the
ROYAL ASTRONOMICAL SOCIETY

MNRAS **452,** 3457–3469 (2015) doi:10.1093/mnras/stv1541

CMB quenching of high-redshift radio-loud AGNs

G. Ghisellini,[1]★ F. Haardt,[2,3] B. Ciardi,[4] T. Sbarrato,[5] E. Gallo,[6] F. Tavecchio[1] and A. Celotti[1,7,8]

[1]*INAF-Osservatorio Astronomico di Brera, Via Bianchi 46, I-23807 Merate, Italy*
[2]*DiSAT, Università dell'Insubria, via Valleggio 11, I-22100 Como, Italy*
[3]*INFN, Sezione di Milano–Bicocca, Piazza della Scienza 3, I-20126 Milano, Italy*
[4]*Max Planck Institute for Astrophysics, Karl–Schwarzschild Strasse 1, D-85741 Garching, Germany*
[5]*Dipartimento di Fisica 'G. Occhialini', Università di Milano–Bicocca, P.za della Scienza 3, I-20126 Milano, Italy*
[6]*Department of Astronomy, University of Michigan, 500 Church St., Ann Arbor, MI 48109, USA*
[7]*Scuola Internazionale Superiore di Studi Avanzati, Via Bonomea 265, I-34135 Trieste, Italy*
[8]*INFN-Sezione di Trieste, via Valerio 2, I-34127 Trieste, Italy*

Accepted 2015 July 7. Received 2015 July 3; in original form 2015 May 19

ABSTRACT

The very existence of more than a dozen of high-redshift ($z \gtrsim 4$) blazars indicates that a much larger population of misaligned powerful jetted active galactic nucleus (AGN) was already in place when the Universe was $\lesssim$1.5 Gyr old. Such parent population proved to be very elusive, and escaped direct detection in radio surveys so far. High-redshift blazars themselves seem to be failing in producing extended radio lobes, raising questions about the connection between such class and the vaster population of radio galaxies. We show that the interaction of the jet electrons with the intense cosmic microwave background (CMB) radiation explains the lack of extended radio emission in high-redshift blazars and in their parent population, helping to explain the apparently missing misaligned counterparts of high-redshift blazars. On the other hand, the emission from the more compact and more magnetized hotspots are less affected by the enhanced CMB energy density. By modelling the spectral energy distribution of blazar lobes and hotspots, we find that most of them should be detectable by low-frequency deep radio observations, e.g. by LOw-Frequency ARray for radio astronomy and by relatively deep X-ray observations with good angular resolution, e.g. by the *Chandra* satellite. At high redshifts, the emission of a misaligned relativistic jet, being debeamed, is missed by current large sky area surveys. The isotropic flux produced in the hotspots can be below $\sim$1 mJy and the isotropic lobe radio emission is quenched by the CMB cooling. Consequently, even sources with very powerful jets can go undetected in current radio surveys, and misclassified as radio-quiet AGNs.

Key words: radiation mechanisms: non-thermal – BL Lacertae objects: general – quasars: general – X-rays: general.

1 INTRODUCTION

Relativistic jets from powerful radio-loud active galactic nuclei (AGNs) carry energy and particles from within the sphere of influence of the central supermassive black hole out to distances that far exceed the size of their host galaxy (e.g. Schoenmakers et al. 2000; de Vries, Becker & White 2006). When the jet interacts with the external medium, a hotspot is formed, powering the extended structures we call 'lobes'. The lobes are characterized by relatively low magnetic fields (tens of μG), and are thus inefficient synchrotron radiators. Minimum energy arguments, based on the assumption of equipartition between the particle and magnetic energies, suggest that the lobes of the most powerful sources can store up to 10^{61} erg in energy.

Even when we do not have (yet) resolved radio maps of the hotspots and of the lobes (e.g. when we have only single dish observations), their presence can be inferred from steep low-frequency radio spectra, characteristic of optically thin synchrotron emission, in contrast to the flat spectra of partially self-absorbed, optically thick jets

Fig. 1 illustrates the point by showing the broad-band spectral energy distribution (SED) of 1224+2122 (a.k.a. 4C + 21.35), a $z = 0.434$ blazar detected in the γ-ray band by the *Fermi* satellite

★ E-mail: gabriele.ghisellini@brera.inaf.it

© 2015 The Authors
Published by Oxford University Press on behalf of the Royal Astronomical Society

Downloaded from https://academic.oup.com/mnras/article-abstract/452/4/3457/1060612 by INAF Brera Milano (Osservatorio Astronomico di Brera) user on 28 February 2020

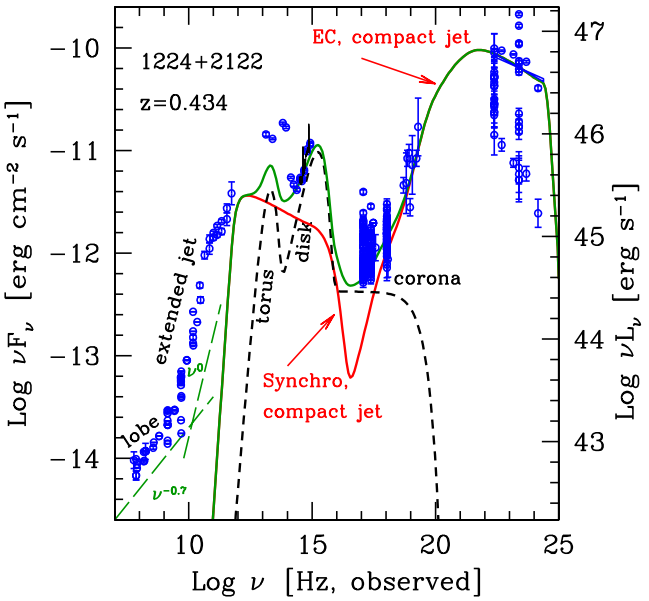


Figure 1. SED of CRATES J1224+2122 (alias PKS 1222+21 alias 4C +21.35), a *Fermi*/Large Area Telescope (LAT) detected blazar (Shaw et al. 2012). The solid red line is the emission from the single-zone jet model we adopted (see text and Ghisellini & Tavecchio 2015), the short-dashed black line is the contribution from the thermal components (i.e. accretion disc, the torus and the X-ray corona), while the solid green line is the sum of the two. The adopted jet model assumes that most of the emission comes from a compact jet region, and therefore the synchrotron emission is self-absorbed up to $\sim 10^3$ GHz. At lower frequencies, the flux is produced by several larger jet regions, self-absorbing at smaller frequencies, and by the extended radio-lobes, whose synchrotron emission is optically thin. The latter component is relatively steep ($F_\nu \propto \nu^{-0.7}$), while the partially opaque emission from the jet is flat ($F_\nu \propto \nu^0$), as illustrated by the long-dashed green lines.

(Ackermann et al. 2011; Shaw et al. 2012).[1] Multiple data points at the same frequency indicate the strong variability typical of blazars, that can reach an amplitude of 1–2 orders of magnitude at X-ray and γ-ray energies, while it is much less extreme in the radio band. The signature of isotropic and optically thin synchrotron emission produced by the hotspots and by the radio lobes is the relatively steep slope of the radio spectrum below a few GHz, $F_\nu \propto \nu^{-0.7} - \nu^{-1.5}$. Above a few GHz the radio spectrum, produced by the partially opaque jet (labelled as 'extended jet' in Fig. 1), is instead much flatter, i.e. $F_\nu \propto \nu^0$. Note that the long-dashed lines at the lowest radio frequencies are not fits to the lobe and extended jet emission. Their purpose here is simply to guide the eye. Note that the case of 1224+2122 is not common, since most blazars do not show the spectral steepening at low radio frequencies, even when going down to 74 MHz, as shown by Massaro et al. (2013).

Whereas the core jet emission is strongly collimated and boosted by relativistic beaming, the hotspot and lobe emission is largely isotropic (or at most mildly beamed). This implies that, as a first approximation, the jet-to-lobe flux ratio (i.e. the so-called core dominance) is an indicator of the observer's viewing angle. For each source whose jet is pointing at an angle $\theta_v \leq 1/\Gamma$ (where Γ is the jet bulk Lorentz factor), and whose power is large enough to produce radio lobes, there must exist $\sim 2\Gamma^2$ sources with strongly misaligned (and thus undetectable) jets, and whose radio lobes should be visible regardless of the viewing angle, given the required instrument sensitivity. If so, then radio galaxies and misaligned radio-loud quasars ought to be $2\Gamma^2$ times more numerous than blazars.

Volonteri et al. (2011) showed that this straightforward prediction is confirmed up to $z \sim 3$, beyond which the number of radio galaxies dramatically drops. More specifically, the expected number density of misaligned radio-loud quasars and radio galaxies as inferred from the *Swift*/Burst Alert Telescope (BAT) sample of luminous, massive blazars (Ajello et al. 2009), overestimates the number of observed luminous, radio-loud AGNs [from SDSS-DR7+Faint Images of the Radio Sky at Twenty-Centimeters (FIRST)] by a factor $\sim$3 in the redshift bin $z = 3$–4, and by a factor >10 between $z = 4$ and 5 (see table 1 and fig. 3 in Volonteri et al. 2011; qualitatively similar conclusions are reached by Kratzer & Richards 2015; see also Haiman, Quataert & Bower 2004; Mc Greer, Helfand & White 2009).

Volonteri et al. (2011) put forward some possible explanations of this discrepancy, namely: (i) heavy optical obscuration of high-z radio galaxies; (ii) substantial drop in the average Γ for high-z sources and (iii) substantial dimming of the radio lobes at $z \gtrsim 3$. The first scenario implies the existence of a large population of infrared-luminous, radio-loud quasars with weak optical counterparts. The second scenario implies a very large density of the emitting relativistic electrons (leading to a very large jet kinetic power; see Ghisellini & Tavecchio 2010).

With respect to the third hypothesis, the idea has long been entertained of cosmic microwave background (CMB) photons affecting the behaviour of jetted AGNs (e.g. Celotti & Fabian 2004).

In a recent work, Ghisellini et al. (2014a) have explored specifically how the interaction between the CMB radiation and electrons within the jet-powered lobes affects the appearance of jetted AGNs at different redshifts. The major results can be summarized as follows: owing to its $(1 + z)^4$ dependence, the CMB energy density $U_{\rm CMB}$ starts to dominate over the magnetic energy density $U_{\rm B}$ within the lobes above $z \simeq 3$, thereby suppressing the synchrotron radio flux at higher z (hereafter referred to as *CMB quenching*). At the same time, high-energy electrons will cool effectively by inverse Compton losses scattering off CMB photons. Combined, these two effects result in a significant enhancement of the diffuse X-ray emission – in the form of X-ray lobes – from high-z quasars (Celotti & Fabian 2004; Mocz, Fabian & Blundell 2011). The hotspot radio emission is less affected by the CMB quenching, since they are more compact and more magnetized than the lobes. However, at low redshifts, their contribution to the total radio flux is less than the contribution due to the radio lobes.

In this paper, we consider all radio-loud sources at $z > 4$ confirmed to be blazars, and construct their broad-band SEDs. These SEDs have all a radio flat spectrum (where flat means $F(\nu) \propto \nu^{-\alpha}$ with $\alpha < 0.4$). This spectrum is produced by different regions of the jet, from the very compact (subparsec) to the extended regions (tens of kpc from the black hole, or more). In all cases, we see no hints of the presence of a steep thin synchrotron component produced by the hotspots and by the radio lobes at (rest-frame) frequencies $\lesssim$1 GHz, hence providing observational support to the CMB quenching scenario for high-z jetted AGNs. By applying a state-of-the-art jet emission model, we will fully characterize the physical properties of the jets. This will allow us to constrain the expected properties of both the hotspots and the lobes, whose broad-band emission can then be modelled under few reasonable assumptions (such as energy equipartition between electrons and magnetic field). Finally, we will address the observability of such low-surface brightness radio lobes from the known population of $z > 4$ blazars at

[1] All shown data points are taken from the ASI Science Data Center (ASDC) archive.

Downloaded from https://academic.oup.com/mnras/article-abstract/452/4/3457/1060612 by INAF Brera Milano (Osservatorio Astronomico di Brera) user on 28 February 2020

Table 1. Our blazar sample, containing all known blazars at $z \geq 4$. Column [1]: right ascension and declination; Column [2]: redshift; Column [3]: flag for belonging to the SDSS + FIRST survey; Column [4]: radio loudness; Column [5]: logarithm of the bolometric luminosity (from S11) Column [6]: logarithm of the CIV emission line luminosity (from S11); Column [7]: black hole mass (in solar masses, best estimate from S11); Column [8]: broad line region luminosity (in units of 10^{45} erg s^{-1}), obtained from CIV; Column [9]: black hole mass (in solar masses) from disc fitting; Column [10]: accretion disc luminosity (in units of 10^{45} erg s^{-1}) from disc fitting; Column [11]: references.

Name [1]	z [2]	SDSS + FIRST [3]	R [4]	$L_{\rm bol}$ [5]	$L_{\rm CIV}$ [6]	$M_{\rm vir}$ [7]	$L_{\rm BLR,45}$ [8]	$M_{\rm fit}$ [9]	$L_{\rm d,45}$ [10]	Ref [11]
032444.30−291821.0	4.630	N	4468	...	...	...	...	5e9	200	Yuan et al. (2006)
052506.18−334305.5	4.413	N	1230	...	...	...	...	3e9	148	Fabian et al. (2001a)
083946.22+511202.8	4.390	Y	285	47.5	45.0	8.9e9	8.8	7e9	178	Bassett et al. (2004); Sbarrato et al. (2013a)
090630.75+693030.8	5.47	N	1000	...	...	...	...	3e9	68	Romani et al. (2004)
102623.61+254259.5	5.304	Y	5200	...	...	...	...	5e9	75	Sbarrato et al. (2012)
102838.80−084438.6	4.276	N	4073	...	...	...	...	4e9	120	Yuan et al. (2000)
114657.79+403708.6	5.005	Y	1700	...	...	...	...	4e9	114	Ghisellini et al. (2014b)
125359.62−405930.5	4.460	N	4700	...	...	...	...	2e9	42	Yuan et al. (2006)
130940.70+573309.9	4.268	Y	133	47.1	45.1	2.1e8	46.0	8e9	57	This paper
132512.49+112329.7	4.412	Y	879	47.4	45.4	2.8e9	46.4	3e9	55	This paper; Sbarrato et al. (2013a)
142048.01+120545.9	4.034	Y	1904	47.1	45.0	1.9e9	8.16	2e9	54	Sbarrato et al. (2015)
143023.7+420436	4.715	Y	5865	...	...	...	...	1.5e9	135	Fabian et al. (2001b)
151002.92+570243.3	4.309	Y	13000	47.1	44.9	3.2e8	6.6	1.5e9	59	Yuan et al. (2006)
171521.25+214531.8	4.011	Y	30000	...	...	...	...	6e8	5.5	Gobeille et al. (2014); Wu et al. (2013)
213412.01−041909.9	4.346	Y	24000	...	...	...	...	1.5e9	101	Sbarrato et al. (2015)
222032.50+002537.5	4.205	Y	4521	46.9	45.1	1.4e9	10.	2e9	45	Sbarrato et al. (2015)

(rest-frame) frequencies at or below the GHz band, specifically with the LOw-Frequency ARray (LOFAR; van Haarlem et al. 2013).

We adopt a cosmology with $\Omega_{\rm m} = 0.3$, $\Omega_\Lambda = 0.7$ and $H_0 = 70$ km s^{-1} Mpc^{-1}.

2 THE BLAZAR SAMPLE

Following Sbarrato et al. (2013a), we consider all 31 spectroscopically confirmed $z > 4$ quasars in the SDSS + FIRST sample owning a radio loudness $R = F_{5\,\rm GHz}/F_{2500\,\text{Å}} > 100$, where $F_{5\,\rm GHz}$ and $F_{2500\,\text{Å}}$ are the monochromatic fluxes at 5 GHz and at 2500 Å, respectively (see Shen et al. 2011, hereafter S11). Six bona-fide blazars (see Table 1) are then identified from this initial sample of 31 sources based on *Swift* X-Ray Telescope (Sbarrato et al. 2012, 2015; Ghisellini et al. 2014b, 2015) and *NuSTAR* follow-up observations (Sbarrato et al. 2013b). Two other quasars out of the 31 had archival X-ray data, showing intense and hard X-ray spectra: by fitting their multiwavelength SEDs, we can now classify SDSS J130940.70+573309.9 and SDSS J132512.49+112329.7 as blazars, thanks to their small viewing angles and high Lorentz factors.

In addition, we include eight other blazars at $z > 4$ (see Table 1) serendipitously identified in X-rays. Among these eight sources, we note that 213412.01−041909.9 is in the SDSS + FIRST sample, but it was not included in the Shen et al. sample because there was no spectroscopic follow-up. A spectroscopic redshift of $z = 4.346$ was determined by Hook et al. (2002) for this source. The same occurs for 143023.7+420436 and SDSS J171521.25+214531.8, whose redshifts ($z = 4.715$ and $z = 4.011$, respectively) were first determined by Hook & McMahon (1998). The latter has a further indication of its orientation given by extended radio emission (Gobeille, Wardle & Cheung 2014).

To summarize, we consider a grand total of 16 blazars with confirmed $z > 4$; 3 of them are at $z > 5$, and 11 objects belong to the SDSS + FIRST sample. In Table 1, we list the main references for each object, while the SEDs are shown in Figs 3 and 8.[2]

[2] Data are taken from the papers listed in Table 1 and from the ASDC archive at http://tools.asdc.asi.it/.

3 EMISSION MODELS

In this section, we summarize the main properties of the models for the jet, the hotspot and lobe emissions we use. Full details can be found in Ghisellini & Tavecchio (2009, for the jet) and in Ghisellini et al. (2014a, for the lobe), and interested readers are referred there.

Modelling the jet emission allows us to estimate the total jet power, which we assume to be conserved along the jet and to power the lobes on a much larger scale. A clear estimate of the jet power is therefore instrumental in modelling the lobe emission. Other important parameters characterizing the lobes, such as the physical extension, the average magnetic field, and the particle energy distribution are, basically, unknown. We assume physically motivated values for them, and discuss how our choices impact on the final results.

3.1 Jet emission

For the jet emission, we adopt a simple, one-zone, leptonic model (Ghisellini & Tavecchio 2009). The model assumes that most of the observed radiation is produced in a single spherical region within a conical jet of semi-aperture $\psi = 0.1$ rad. The spherical region is initially located at a distance $R_{\rm diss}$ from the black hole, it is homogeneously filled with a tangled magnetic field B, and it moves with velocity βc, corresponding to a bulk Lorentz factor Γ, at an angle $\theta_{\rm v}$ with respect to the line of sight. The resulting Doppler factor is $\delta = 1/[\Gamma(1 - \beta\cos\theta_{\rm v})]$. Relativistic electrons are injected throughout the spherical region at a constant rate $Q(\gamma)$, with total *comoving* power (i.e. as measured in the jet comoving frame)

$$P'_{\rm e} = V m_{\rm e} c^2 \int_{\gamma_{\rm min}}^{\gamma_{\rm max}} Q(\gamma)\gamma\,{\rm d}\gamma, \quad (1)$$

where V is the volume of the emitting region and $\gamma_{\rm min}$ and $\gamma_{\rm max}$ are the minimum and maximum injection energies. The electron energy distribution $Q(\gamma)$ is taken as a smoothly connected double power

Downloaded from https://academic.oup.com/mnras/article-abstract/452/4/3457/1060612 by INAF Brera Milano (Osservatorio Astronomico di Brera) user on 28 February 2020

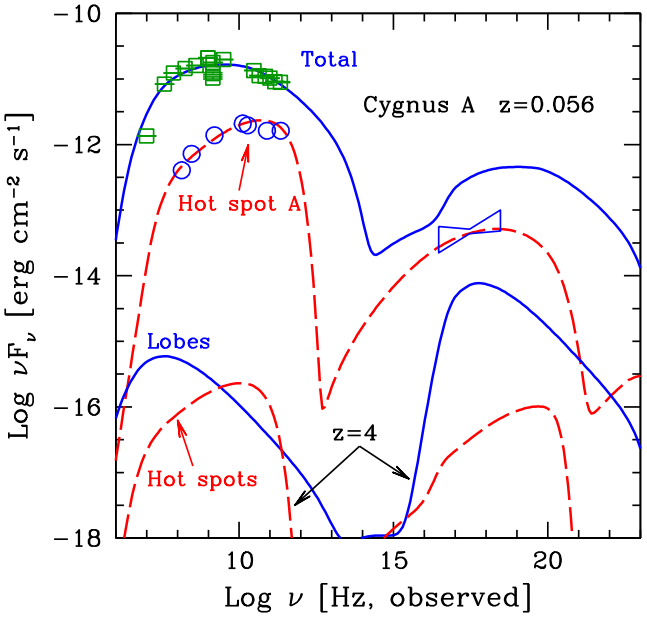


Figure 2. SED of the hotspot A (the brightest) of Cygnus A (blue circles), compared to the total radio emission (green squares). The blue bow tie refers to the X-ray flux of the hotspot A as observed by *Chandra* (Wilson et al. 2000). The dashed red and solid blue lines are the corresponding SSC models. For simplicity, we have fitted the total emission with the lobe model. The bottom lines show how the emission of the lobes and the hotspots would appear if the source were at $z = 4$.

law, with slopes s_1 and s_2 below and above the break energy $\gamma_{\rm b}$, respectively:

$$Q(\gamma) = Q_0 \frac{(\gamma/\gamma_{\rm b})^{-s_1}}{1+(\gamma/\gamma_{\rm b})^{-s_1+s_2}} \quad ({\rm cm}^{-3}{\rm s}^{-1}). \tag{2}$$

In the following, we will assume that $s_1 \leq 1$, $s_2 > 2$ and $\gamma_{\rm min} = 1$. For this choice of s_2, the exact value of $\gamma_{\rm max}$ is not critical, since it corresponds to the end of the steep tails of both the synchrotron and the inverse Compton spectrum. Having specified the injection term, the particle density distribution $N(\gamma)$ (cm^{-3}) is found by solving the continuity equation at a time equal to the light crossing time (that is also the time-scale for doubling the source size), taking into account radiative cooling and electron–positron pair production. Additionally, we consider the presence of a standard, optically thick, geometrically thin accretion disc (Shakura & Sunyaev 1973), assumed to emit a total luminosity $L_{\rm d} = 10^{45} L_{\rm d,45}$ erg s^{-1}. The assumption of a moving blob may correspond to the 'internal shock' scenario, in which two shells, initially separated by some distance ΔR, move with different Γ and collide at a distance $\approx \Gamma^2 \Delta R$ from the black hole (Rees 1978; Ghisellini 1999; Spada et al. 2001). Calculating the particle distribution at the light crossing time, when the particle injection stops, corresponds to the maximum produced flux, and allows to neglect adiabatic losses, and changes in the size, magnetic field and particle density of the blob.

We further assume that a broad line region (BLR), responsible for reprocessing 10 per cent of $L_{\rm d}$, lies at a distance $R_{\rm BLR} = 10^{17} L_{\rm d,45}^{1/2}$ cm. Further out, at $R = 2.5 \times 10^{18} L_{\rm d,45}^{1/2}$ cm, a molecular torus intercepts and re-emits a fraction (~20–40 per cent) of $L_{\rm d}$ in the infrared band.

We consider the following emission processes within the jet: (i) synchrotron; (ii) synchrotron self-Compton (SSC) and (iii) inverse Compton of the relativistic electrons scattering off photons produced by the disc, the BLR and the dusty torus (collectively dubbed EC, for external Compton). Photon–photon interactions and pair production are also accounted for, albeit these processes turn out to be unimportant for our blazar sample, which is uniformly characterized by a steep γ-ray spectrum.

The source size $\psi R_{\rm diss}$ is constrained by: (i) the minimum variability time-scale $t_{\rm var}$, as the size must be smaller than $\sim c\, t_{\rm var} \delta/(1+z)$; (ii) the inverse Compton to synchrotron luminosity ratio, which is a function of $R_{\rm diss}$ (see Ghisellini & Tavecchio 2009) and (iii) the location of the peak frequency of the Compton component, which, in turn, dictates the nature of the primary seed photons (i.e. IR from the torus versus UV from the broad lines).

The resulting source size is too compact to account for the observed radio emission, since synchrotron radiation is self-absorbed up to (observed) frequencies $\sim 10^3$ GHz. At lower frequencies, the observed flat radio spectrum ($F_\nu \propto \nu^{-\alpha}$, with $\alpha < 0.4$, and often $\alpha \sim 0$) is understood to be produced by the superposition of the emission from several, larger, parts of the jet. We do not aim to model this part of the spectrum, and in all SEDs shown in Figs 1–6 the long-dashed lines corresponding to $F_\nu \propto \nu^0$ or to

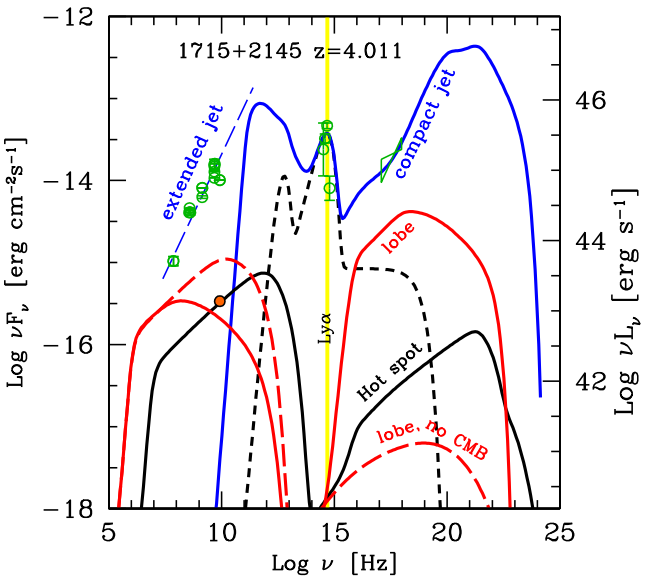


Figure 3. SED of 1715+2145, together with the models for the different components of the emission: (i) the thermal component, namely the accretion disc, the torus and the X-ray corona (short-dashed black line); (ii) the emission from the compact and relativistically beamed jet (the blue solid line is the sum of the jet and the thermal components), accounting for most of the emission, but not for the radio flux, that must be produced by more extended regions (but still relativistic) of the jet, forming the flat radio spectrum; (iii) the emission from the hotspots (solid black line) assumed to have a radius of $R_{\rm spot} = 1.5$ kpc, as measured by VLA (Gobeille et al. 2014); (iv) the lobe emission (solid red line), assuming that the power injected throughout the lobe in the form of relativistic electrons is $P_{\rm e,lobe} = 0.1\, P_{\rm jet}$. Magnetic and electron lobe energies are in equipartition. For illustration, the dashed red line shows the lobe emission for the same $P_{\rm e,lobe}$ and magnetic field, but now neglecting the effects of CMB photons. The long-dashed blue line is not a fitting model, but simply a line to guide the eye. See Table 2 for the adopted parameters. Data points are from the ASDC archive, the bow tie in X-rays is from Wu et al. (2013). The orange circle corresponds to 4 mJy at 8.4 GHz, and is the flux observed by the two hotspots. The vertical yellow line flags the position of the Lyα line. Above this line the flux is severely absorbed by the intervening matter, and we do not consider the corresponding data in the fit. (see for illustration the case of 1026+2542 in Fig. 8).

Downloaded from https://academic.oup.com/mnras/article-abstract/452/4/3457/1060612 by INAF Brera Milano (Osservatorio Astronomico di Brera) user on 28 February 2020

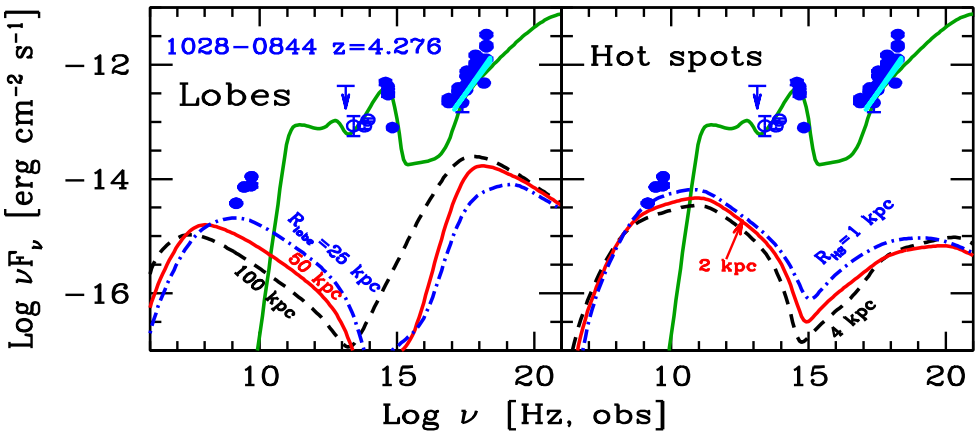


Figure 4. Predicted lobe and hotspot emission from the blazar 1028−0844. The left-hand panel shows the lobe emission for $R_{\rm lobe} = 100$ kpc (short-dashed black line), $R_{\rm lobe} = 50$ kpc (solid red) and $R_{\rm lobe} = 25$ kpc (dot–dashed blue). For all cases, we have assumed that the jet deposits in relativistic electrons the same power, i.e. $0.1P_{\rm e}^{\rm jet} = 2.7 \times 10^{46}$ erg s^{-1} for each lobe and hotspot. For the right-hand panel, the hotspot radius $R_{\rm HS} = 4$ kpc (dashed black line), $R_{\rm HS} = 2$ kpc (solid red) and $R_{\rm HS} = 1$ kpc (dot–dashed blue). The magnetic field is found imposing equipartition with the total electron energy, both for the lobe and for the hotspot. The green solid line refers to the jet model (as in Figs 5 and 6). See Table 2 for the adopted parameters.

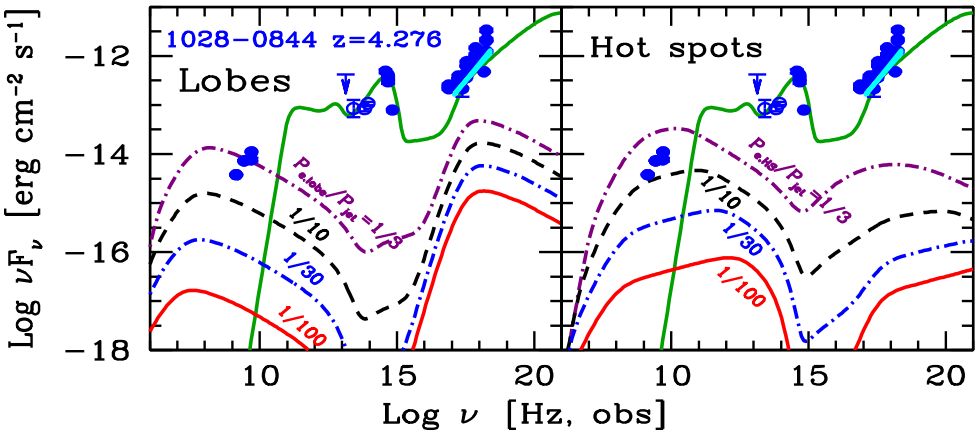


Figure 5. Predicted lobe and hotspot emission from the blazar 1028−0844 as a function of the injected power in relativistic electrons. For both panels $P_{\rm e}/P_{\rm jet} = 1/3$ (violet dot–dashed line); 1/10 (dashed black line); 1/30 (dot–dashed blue line) and 1/100 (solid red line). For all cases, we have assumed that the lobe radius is 50 kpc and the hotspot radius is 2 kpc. The magnetic field is found imposing equipartition with the total electron energy. A larger $P_{\rm e}$ implies a larger equipartition magnetic field and this in turn implies that the synchrotron luminosity increases more than the inverse Compton one. See Table 2 for the adopted parameters.

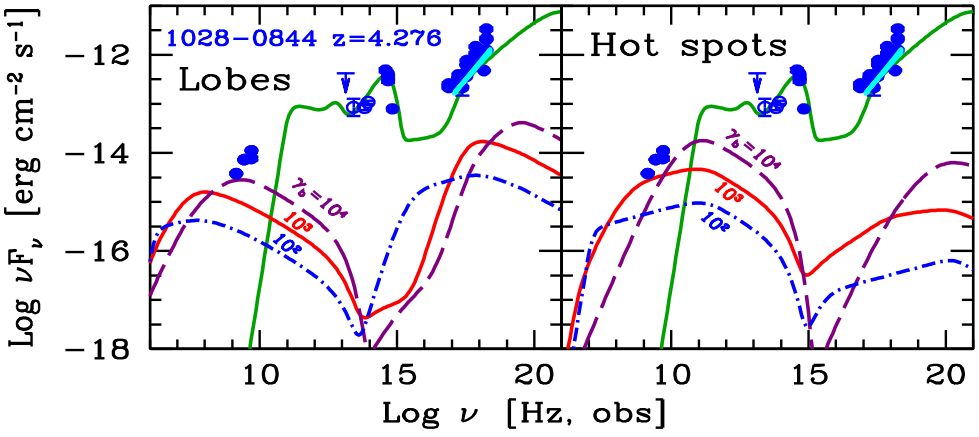


Figure 6. Predicted lobe and hotspot emission from the blazar 1028−0844 as a function of the break energy of the injected electrons $\gamma_{\rm b}$ (see equation 2). For both panels: $\gamma_{\rm b} = 10^4$ (long-dashed violet line); $\gamma_{\rm b} = 3 \times 10^3$ (solid red line); $\gamma_{\rm b} = 3 \times 10^2$ (dot–dashed blue line). For all cases, we have assumed that the lobe radius is 50 kpc and the hotspot radius is 2 kpc. The magnetic field is found imposing equipartition with the total electron energy. See Table 2 for the adopted parameters.

Downloaded from https://academic.oup.com/mnras/article-abstract/452/4/3457/1060612 by INAF Brera Milano (Osservatorio Astronomico di Brera) user on 28 February 2020

$F_\nu \propto \nu^{-1/3}$ simply guide the eye. The outer jet, responsible for the radio spectrum, can be safely neglected because the corresponding luminosity is only a small fraction of the total, and therefore we can assume that the jet retains the bulk of its power up to the lobe site. The magnetic field of the extended part of the jet, up to the kpc size, should be large enough to be unaffected by the CMB quenching: assuming a jet at $z \sim 4$ with $B \sim 1$ G at a distance $d \sim 10^{18}$ cm and $B \propto d^{-1}$, we have that the jet magnetic field starts to be smaller than $B_{\rm CMB}$ for $d > 0.4/(\Gamma/10)$ kpc, where $B_{\rm CMB}$ is the magnetic field in equipartition with the CMB (as seen in the comoving frame of the jet) given in equation (4). If we further assume that the self-absorption frequency of the different jet components scales as d^{-1}, we expect that CMB will reduce the synchrotron flux produced by the extended part of the jets for $\nu \lesssim 250$ MHz. This crude estimate shows that the jet emission remains unaltered at all but the very small frequencies.

The jet carries power in various forms, all of which can be conveniently expressed as energy fluxes as

$$P_{\rm i} = \pi R^2 \Gamma^2 \beta c\, U'_{\rm i}. \quad (3)$$

Here, $U'_{\rm i}$ represents the energy density (in the jet comoving frame) in radiation, $U'_{\rm r}$, corresponding to the radiative jet power $P_{\rm r}$ and in magnetic field, $U'_{\rm B} = B'^2/(8\pi)$, corresponding to the jet Poynting flux $P_{\rm B}$. Finally, we need to consider the kinetic energy density of the electrons, $U'_{\rm e} = m_{\rm e}c^2 \int N(\gamma)\gamma {\rm d}\gamma$, corresponding to the power carried by the electrons, $P_{\rm e}$, and protons, $P_{\rm p}$ (we are assuming to have one cold proton – i.e. whose kinetic energy is due to bulk motion only – per emitting electron). The total jet power, $P_{\rm jet}$, is the sum of all these components.

3.2 Hotspot emission

Powerful jets deposit their kinetic energy into the intergalactic medium through a termination shock, the hotspot, which in turn injects the power received by the jet into the extended lobe structure. To find out the main properties of the hotspot emission, we will examine first the hotspot properties of the closest powerful Fanaroff–Ryley II (FR II) radio galaxy, namely Cygnus A. Then we will interpret the small, but resolved, radio emission of the distant blazar SDSS J171521.25+214531.8 (1715+2145 hereafter) as due to the hotspot emission, to check that if the properties of nearby and distant hotspots are similar for similar jet power.

The radio luminosity of the hotspots of Cygnus A is a factor 5–10 smaller than the radio luminosity of its lobes (Wilson, Young & Shopbell 2000; see Fig. 2). The detection of the hotspots in X-ray by the *Chandra* satellite allowed Wilson et al. (2000) to estimate the magnetic field of the hotspot, $B \sim 1.5 \times 10^{-4}$ G, a value close to equipartition with the emitting electrons. The corresponding magnetic energy density is ∼2000 times larger than the CMB energy density at the redshift $z = 0.056$ of Cygnus A. The magnetic field in equipartition with the CMB energy density, $B_{\rm CMB}$ is

$$B_{\rm CMB} = 3.24 \times 10^{-6}\, \Gamma\, (1+z)^2 = 8.1 \times 10^{-5}\, \Gamma \left(\frac{1+z}{5}\right)^2 {\rm G}, \quad (4)$$

where the Γ factor accounts for the possibility to have a relativistically moving source that would see the CMB energy density amplified by a factor Γ^2. If the magnetic field of the hotspots remains $B \sim 10^{-4}$ G at any redshift, the corresponding magnetic energy density is larger than the radiation energy density of the CMB up to $z \sim 4.5$. Consequently, below this redshift, the effects of the CMB on the radio emission of the hotspots are weak.

To model the emission of both the hotspot and the lobe, we have followed the prescriptions of Ghisellini et al. (2014a) that will be summarized in the next section. To fit the hotspots of Cygnus A, we used $B = 1.1 \times 10^{-4}$ G, an injected power of relativistic electrons $P_{\rm e} = 7 \times 10^{45}$ erg s^{-1} and a radius of 2 kpc. The corresponding magnetic energy is $E_{\rm B} =$ erg, a factor 3.8 smaller than the electron energy $E_{\rm e} = 1.6 \times 10^{57}$ erg. For the lobe emission, we have used $B = 2 \times 10^{-5}$ G, same $P_{\rm e}$ and a lobe radius of 58 kpc. Magnetic and electron energies are the about the same, $E_{\rm B} \sim E_{\rm e} = 3 \times 10^{59}$ erg.

Fig. 2 shows how the SED of the lobe and hotspot emission of Cygnus A would look like if the source were at $z = 4$. The shape (and the luminosity) of the hotspot would remain unaltered, since the total radiative cooling would be dominated by synchrotron losses even at this redshift. Its flux would be fainter only because of the larger distance. On the contrary, the lobe radio spectrum would become much steeper, and thus fainter than the hotspot emission, due to the enhanced inverse Compton radiative cooling, now dominating over synchrotron losses. The enhanced inverse Compton losses produce a correspondingly enhanced X-ray luminosity.

Among the blazars of our sample, 1715+2145, at $z = 4.011$, was observed by the Very Large Array (VLA) by Gobeille et al. (2014), who report the detection of the source at the level of 387 mJy at 8.4 GHz. Most of this total flux (383 mJy) comes from the unresolved core, while the remaining 4 mJy are produced by two almost co-aligned sources of sizes (i.e. diameters) 0.5 ± 0.1 and 0.4 ± 0.1 arcsec, corresponding to 3.5 ± 0.7 and 2.8 ± 0.7 kpc. We interpret them as being hotspots, given the similarity of their sizes with the size of the hotspots observed in Cygnus A. For simplicity, we assume that both hotspots have a radius of 1.5 kpc, and that they contribute 2 mJy each to the observed flux. The power of each jet is $P_{\rm jet} = 1.4 \times 10^{47}$ erg s^{-1}, and we assumed that the power in relativistic electrons injected throughout one hotspot is 10 per cent of $P_{\rm jet}$. To reproduce the observed flux with these assumptions, the magnetic field in the hotspot must be 190 μG. This is not far from equipartition with the emitting electrons, since the corresponding magnetic and electron energies are $E_{\rm B} = 6 \times 10^{56}$ erg and $E_{\rm e} = 1.4 \times 10^{57}$ erg. Fig. 3 shows the SED of the source together with the assumed models for the jet, the hotspots and the lobes (for the latter see below). The hotspot luminosity is a small fraction of the power injected throughout the hotspot in relativistic electrons: in 1715+2145 the hotspot emits about 10^{45} erg s^{-1}, to be compared to $P_{\rm e,HS} = 1.4 \times 10^{46}$ erg s^{-1}. As a consequence, we will assume that the power in relativistic electrons injected throughout the hotspot and the lobe is the same ($P_{\rm e,HS} = P_{\rm e,lobe}$). Since the magnetic field of the hotspots is large, their radio emission is unaffected by the CMB, and remains the same when switching it off.

3.3 Lobe emission

Theoretical models of jet-powered radio lobes rely on high-resolution numerical magneto-hydrodynamic simulations. A crucial role in dictating lobe formation and evolution is played by the environment in which they develop (see e.g. Hardcastle & Krause 2014 for state-of-the-art simulations and references). While low-z radio galaxies inhabit well-known astrophysical environments, such as poor galaxy clusters, the boundary conditions for the high-z jets we are interested in are poorly known at best. As a consequence, we have to rely on numerical work and/or the observed blazar SEDs

Downloaded from https://academic.oup.com/mnras/article-abstract/452/4/3457/1060612 by INAF Brera Milano (Osservatorio Astronomico di Brera) user on 28 February 2020

themselves to estimate some of the fiducial values for modelling the lobe emission.

Following Ghisellini et al. (2014a), we assume a spherical emitting region of radius $R_{\rm lobe}$, which is homogeneously filled with a magnetic field with a coherence length-scale $\lambda = 10$ kpc (see Carilli & Taylor 2002; Celotti & Fabian 2004). Relativistic electrons are injected into the lobe with a total power $P_{\rm e,\,lobe}$ and a distribution with the same functional form $Q(\gamma)$ of equation (2) (but with parameters different from the jet ones). We are assuming that the jet power is essentially constant all along its length, since the radiated power is estimated to be $\sim$10 per cent of $P_{\rm jet}$ (Nemmen et al. 2012; Ghisellini et al. 2014c). The steady-state electron energy distribution is found by solving the continuity equation at particle crossing time $t_{\rm cross} = (R_{\rm lobe}/c)(1 + R_{\rm lobe}/\lambda)$.

Fig. 3 shows the SED of 1715+2145 and the lobe model assuming $P_{\rm lobe} = 0.1\ P_{\rm jet} = 1.4 \times 10^{46}$ erg s^{-1}, a size $R_{\rm lobe} = 50$ kpc, and equipartition between relativistic electrons and magnetic field, giving $B = 20$ μG for the lobe. For comparison, we show how the lobe emission would look like by neglecting the interaction of electrons with the CMB. The CMB enhances the X-ray emission by $\simeq$2 orders of magnitude, while dimming the radio emission at frequencies $\gtrsim$100 MHz. The lobe emission at lower ν is instead not CMB-quenched. This happens because low-energy electrons, responsible for the radio flux at $\nu \lesssim 100$ MHz, do not have enough time to cool, even considering the extra losses due to the interactions with CMB photons. Their number, obtained from the continuity equation, is not controlled by the cooling rate, rather it simply equals the injection rate multiplied by the time elapsed from the start of the injection (see Ghisellini et al. 2014a for full details).

3.3.1 *Constraints on the physical parameters of the hotspot and lobe*

In this part of the section, we discuss the constraints we can put on the physical parameters of the hotspot and lobe, and how the predicted spectrum depends upon the assumed values. To this aim we consider one particular blazar in our sample, namely 1028−0844. In all tested models, the magnetic field is estimated by requiring equipartition with the electron total energy. Equipartition is actually supported by observations of classical double FR II radio galaxies in the radio and X-ray bands, and appears as an educated guess (Wilson et al. 2000; Croston et al. 2004, 2005; Belsole et al. 2004).

Size. The radius of the hotspots of the nearby radio-galaxy Cygnus A and of the distant blazars 1715+2145 is close to 2 kpc for both sources. In Fig. 4 (right-hand panel), we show the emission assuming $R_{\rm HS}$ =1, 2 and 4 kpc, always requiring equipartition between the magnetic and electron energy densities. One can see that the hotspot emission is not sensitive to the changes in size. The assumption $P_{\rm e,HS} = 0.1\ P_{\rm jet}$, for this particular source, leads to an overestimation of the observed radio spectrum, once the hotspot emission is summed to the flat radio emission of outer parts of the jet. The synchrotron luminosity dominates over the inverse Compton one, and their sum is a small fraction of $P_{\rm e,HS}$.

At low redshift, radio lobes form in the overdense environment appropriate for a galaxy cluster. However, at $z \gtrsim 4$ clusters have to form yet, and we can argue that lobes of radio galaxies develop within a medium at (or close to) the mean cosmic density. It turns out that at $z \simeq 4$ the mean cosmic density is comparable to the typical density of the intra-cluster medium $\simeq$1 Mpc away from the centre of a typical formed cluster at $z \lesssim 1$. Because of this coincidence, we then expect that the lobe sizes of high-redshift blazars are not very different from those of very powerful radio sources residing in low-z virialized clusters (although some additional effect may cause the apparent lack of hotspots and lobes at distances larger than 100 kpc for FR II radio galaxies at $z \gtrsim 1$ found by van Velzen, Falcke & Körding 2015).

Table 2. Model parameters for the lobe (top part) and host spot (bottom part) emission of 1028−0844 ($z = 4.276$). For all models, we assumed $s_1 = -1$, $s_2 = 2.7$ and $\gamma_{\rm max} = 10^6$. Column [1]: dimension of the emitting zone in kpc; Column [2]: power injected in each hotspot and lobe in the form of relativistic electrons in units of 10^{45} erg s^{-1}; Column [3]: magnetic field in μG; Column [4]: break Lorentz factors of the injected electron distribution; Columns [5] and [6]: logarithm of the magnetic and electron energy contained in the hotspot or in the lobe in units of erg; Column [7]: figure where the model is shown.

$R_{\rm lobe}$ [1]	$P_{\rm e,lobe,45}$ [2]	$B_{\mu\ \rm G}$ [3]	$\gamma_{\rm b}$ [4]	$\log E_{\rm B}$ [5]	$\log E_{\rm e}$ [6]	Fig. [7]
50	27	24.5	1e3	59.56	59.57	4, 5, 6
25	27	40.1	1e3	59.10	59.10	4
100	27	17.0	1e3	60.15	60.14	4
50	82	42.5	1e3	60.04	60.04	5
50	9	14.1	1e3	59.08	59.09	5
50	2.7	7.8	1e3	58.57	58.57	5
2	27	21.2	1e4	59.44	59.43	6
2	27	27.4	1e2	59.66	59.66	6
$R_{\rm HS}$ [1]	$P_{\rm e,HS,45}$ [2]	$B_{\mu\rm G}$ [3]	$\gamma_{\rm b}$ [4]	$\log E_{\rm B}$ [5]	$\log E_{\rm e}$ [6]	Fig. [7]
2	27	310	1e3	57.58	57.57	4, 5, 6
1	27	585	1e3	57.22	57.23	4
4	27	170	1e3	57.96	57.95	4
2	90	540	1e3	58.06	58.06	5
2	9	180	1e3	57.11	56.11	5
2	2.7	97	1e3	56.57	56.57	5
2	27	95	1e4	56.55	56.55	6
2	27	98	1e2	56.58	56.57	6

The left-hand panel of Fig. 4 shows the predicted lobe emission assuming different values of $R_{\rm lobe}$. Different values of $R_{\rm lobe}$ lead to different values of the equipartition magnetic field (see the values in Table 2) and hence of the self-absorption synchrotron frequency. Therefore, although the power injected in the lobes is fixed, the synchrotron luminosity gets smaller for larger $R_{\rm lobe}$ as this corresponds to a smaller magnetic field. The X-ray luminosity is instead nearly independent upon $R_{\rm lobe}$, because in the fast cooling regime (i.e. when most electrons with $\gamma > \gamma_{\rm b}$ cool radiatively) the emitted power balances the (assumed constant) injected power. Fig. 4 indicates that, under our assumptions, $R_{\rm lobe}$ has to be $\gtrsim$25 kpc to keep model predictions consistent with the observed SED.

Injected power in relativistic electrons. We assume that the power injected in relativistic electrons throughout the hotspot and the lobe is a fraction of the total jet power $P_{\rm jet}$. The value of this fraction is basically unknown, but we can set $P_{\rm e,HS} = P_{\rm e,\,lobe}$ since radiative losses are not important in the hotspot.

If magnetic field, proton energy and electron energy are in equipartition and in addition we account for the pV work of the lobe, then $\sim$10 per cent appears a fair guess. On the other hand, recent numerical work by Hardcastle & Krause (2014, see their fig. 5), suggests a value close to 1 per cent (characteristic of an environment where hot protons dominate the global energetics).

The right-hand panel of Fig. 5 shows how the emission from the hotspots changes by changing $P_{\rm eHS}$. For $P_{\rm e,\,HS} = 10^{-2} P_{\rm jet}$ the

Downloaded from https://academic.oup.com/mnras/article-abstract/452/4/3457/1060612 by INAF Brera Milano (Osservatorio Astronomico di Brera) user on 28 February 2020

corresponding magnetic field is relatively small, and most electrons do not cool while crossing the hotspot. As a consequence the particle distribution does not steepen because of cooling, and the spectrum is hard. As $P_{\rm e,\,HS}$ increases, also the equipartition magnetic field increases (see Table 2), together with the cooling rate, inducing a steepening in the particle distribution and in the produced spectrum.

The left-hand panel of Fig. 5 illustrates the effect of changing $P_{\rm e,\,lobe}$ while keeping $R_{\rm lobe} = 50$ kpc and the magnetic field in equipartition with the total electron energy. This forces the synchrotron luminosity to increase as approximatively $\propto P^2_{\rm e,lobe}$, since a larger $P_{\rm e,\,lobe}$ implies a higher electron density *and* a higher value of the equipartition magnetic field. By comparing the different models in Fig. 5, we conclude that, unless $R_{\rm lobe} \gg 50$ kpc, assuming $P_{\rm e,\,lobe}$ in excess of 10 per cent $P_{\rm jet}$ leads to an overestimate of the radio emission.

Break energy of the injected electrons. Fig. 6 illustrates the effects of varying the electron energy at the break of the energy distribution (equation 2). An increase of $\gamma_{\rm b}$ corresponds to an increase in the power injected in high-energy electrons (which cool more efficiently). This translates into a higher bolometric luminosity and a reduced total energy. This is true both for the hotspot and the lobe. Higher values of $\gamma_{\rm b}$ also correspond to a larger Compton dominance, with the inverse Compton spectrum peaking at larger frequencies. We can now summarize our fiducial values for the hotspot and the lobe parameters. We will assume all sources have hotspots of size $R_{\rm HS}$ =2 kpc, and that $P_{\rm e,HS} = P_{\rm e,lobe} = 0.1$ $P_{\rm jet}$ and $P_{\rm e,HS} = P_{\rm e,lobe} = 0.01$ $P_{\rm jet}$. We will assume equipartition between the magnetic field and the total electron energy, while for the injected particle distribution (i.e. equation 2) we will take power-law indices $s_1 = -1$ and $s_2 = 2.7$, and break and maximum Lorentz factor $\gamma_{\rm b} = 10^3$ and $\gamma_{\rm max} = 10^6$, respectively. As mentioned, the steep value of s_2 makes the exact value of $\gamma_{\rm max}$ not critical.

4 RESULTS

The jet, hotspot and lobe modelling described in the previous sections are applied to the broad-band SEDs of our sample of high-z blazars. In Figs 7 and 8, we show the observed SEDs, along with the corresponding jet and hotspot + lobe emission models. Models of hotspot and lobe emission take into account the CMB when solving for the electron radiative cooling, and for the resulting energy distribution and emitted spectrum.

The parameters required to describe the SED from mm to hard X-ray bands are listed in Tables 3 and 4, while the derived black hole masses and accretion disc luminosities are reported in Table 1. Quite remarkably, the resulting best-fitting parameters of the jet are very similar to what found for the much larger sample of *Fermi*/LAT blazars analysed by Ghisellini & Tavecchio (2015) and Ghisellini et al. (2014c), though none of our high-z blazars has been actually detected by *Fermi*/LAT at γ-ray energies.

Typical sizes for the dissipation region are in the range (3–15) $\times$ 10^{17} cm, which lies within the BLR (except in the case of 0839+5112, for which $R_{\rm diss}$ is slightly larger). The jet magnetic field is found to be $\sim$1–2 G, the bulk jet Lorentz factor $\Gamma \sim 13$–15, and the jet power $46.4 < \log(P_{\rm jet}/{\rm erg\,s^{-1}}) < 47.9$.

Once that data are fitted to the composite jet/disc/torus model, we can estimate the physical parameters of the hotspot and lobe. Assuming $P_{\rm e}/P_{\rm jet} = 0.1$, the equipartition magnetic field is estimated to be between 82 and 510 μG for the hotspots and between

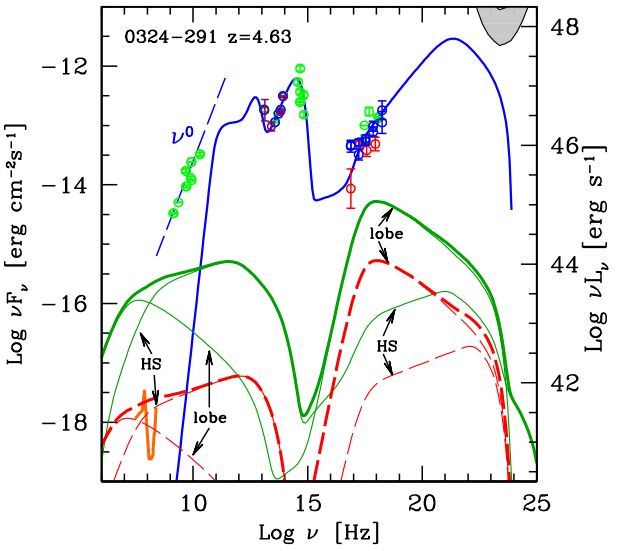


Figure 7. SED of the blazar 0324−291. The blue solid line is the model for the sum of jet emission and thermal components (see Fig. 1). For the hotspots and the lobes, we show two possible models: one with 0.1 $P_{\rm jet}$ (thin green lines) and the other with 0.01 $P_{\rm jet}$ (thin red lines). We show separately the contribution of the hotspots and the lobes, as labelled, while the thick green and red lines are the corresponding sums. The radius of the hotspots and the lobes are assumed to be $R_{\rm HS} = 2$ kpc and $R_{\rm lobe} = 50$ kpc. The straight dashed blue line interpolating the radio spectrum is not a fit, but only a guide to the eye. The hatched grey area in the upper right corner shows the sensitivity of *Fermi*/LAT (5σ) after 5 yr of observing time. We also report (orange line) the sensitivity of LOFAR.

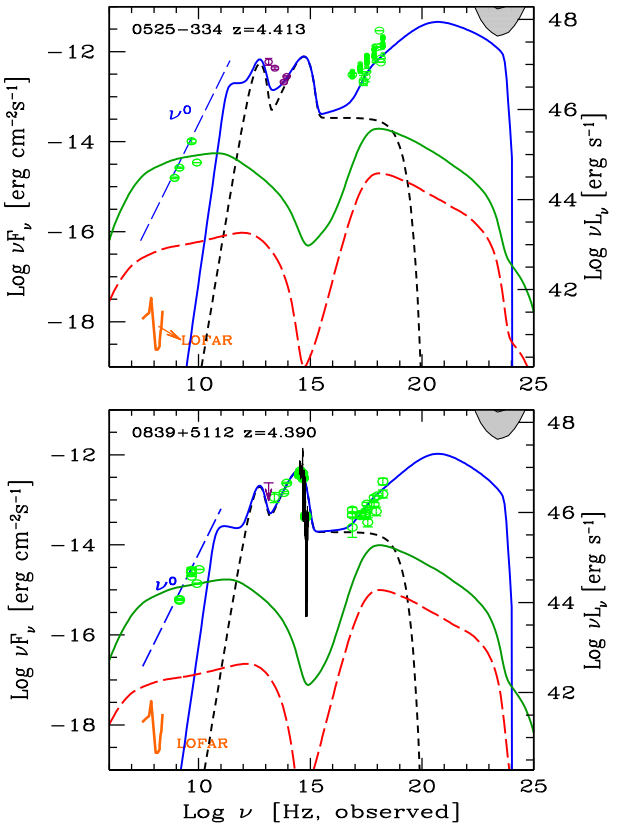


Figure 8. SED of the $z > 4$ blazars. As in Fig. 7, but showing only the sum of the hotspot and lobe components. For 0839+5112, the black solid line shows the SDSS spectrum dereddened for Galactic absorption.

Downloaded from https://academic.oup.com/mnras/article-abstract/452/4/3457/1060612 by INAF Brera Milano (Osservatorio Astronomico di Brera) user on 28 February 2020

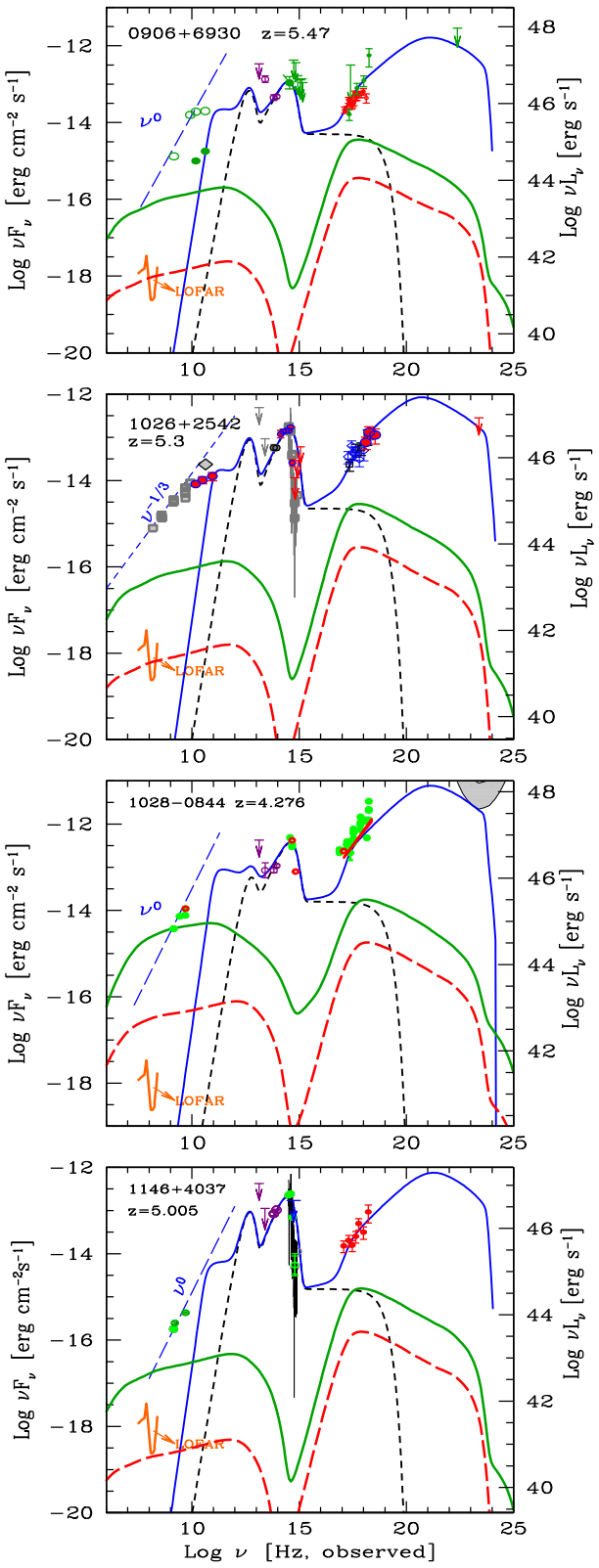


Figure 8 – *continued*

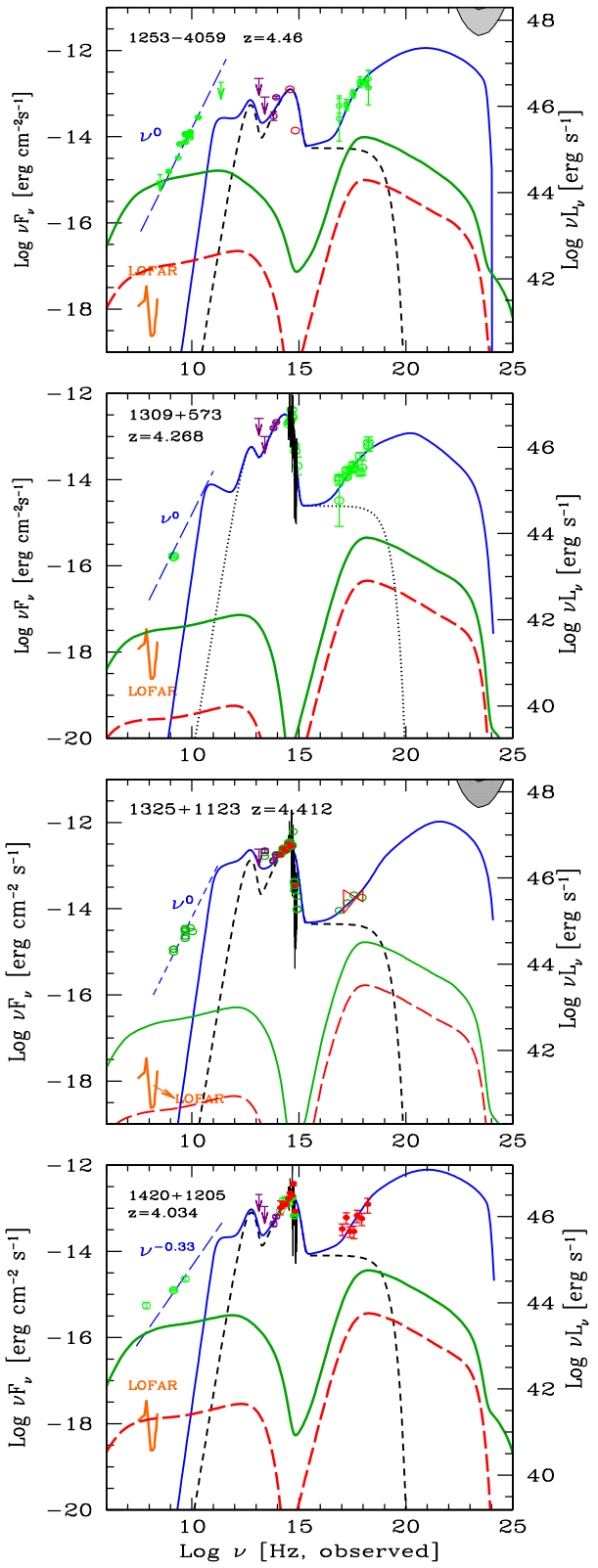


Figure 8 – *continued*

Downloaded from https://academic.oup.com/mnras/article-abstract/452/4/3457/1060612 by INAF Brera Milano (Osservatorio Astronomico di Brera) user on 28 February 2020

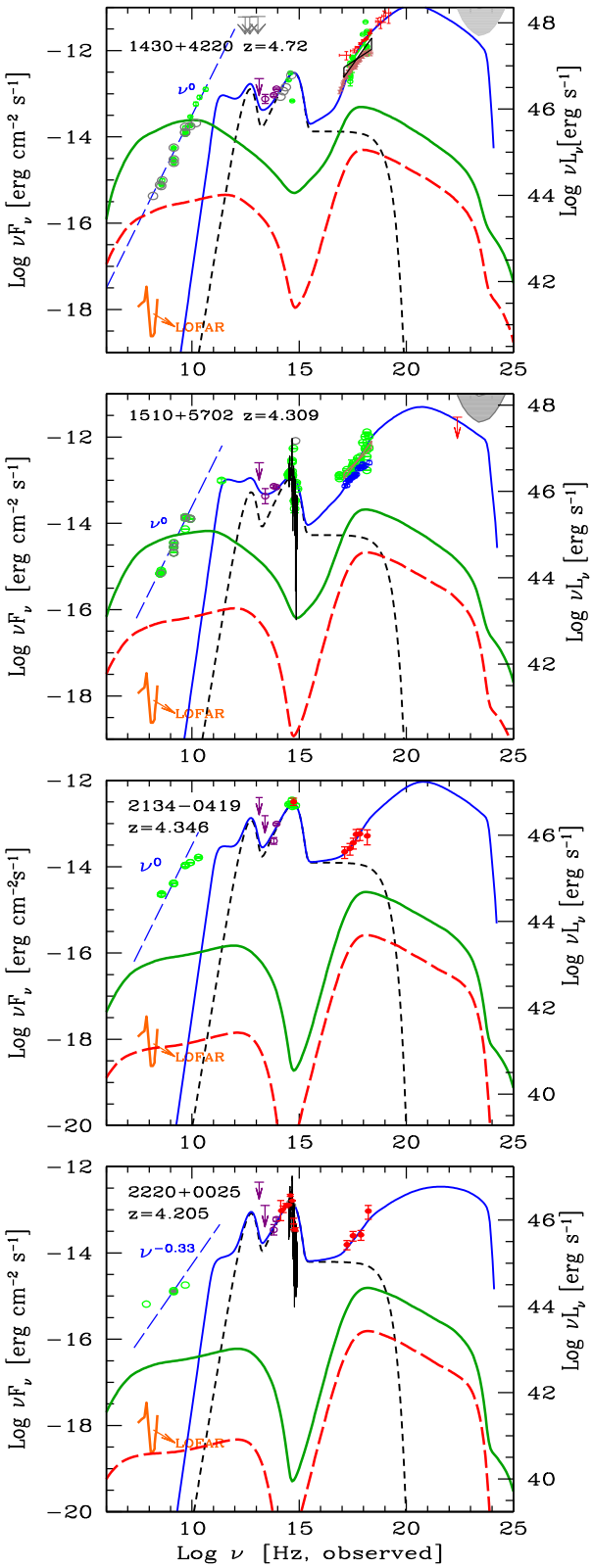


Figure 8 – *continued*

7 and 41 μG for the lobes, while the total energies range from $\log(E_B/\mathrm{erg}) = \log(E_e/\mathrm{erg}) = 56.1$ to 58 for the hotspots and $\log(E_B/\mathrm{erg}) = \log(E_e/\mathrm{erg}) = 58.5$ to 60 for the lobes. For the $P_{e,lobe}/P_{jet} = 10^{-2}$ case, we find B_{HS} between 16.5 and 169 μG, B_{lobe} between 2.3 and 13 μG, and $\log(E_B/\mathrm{erg}) = \log(E_e/\mathrm{erg})$ between 55 and 57 for the hotspots and between 57.5 and 59 for the lobes.

The calculated hotspot + lobe emission, for $P_{e,lobe}/P_{jet} = 0.1$, sometimes exceeds the observed data, requiring that less power is deposited into the hotspots and the lobes. For $P_{e,lobe}/P_{jet} = 10^{-2}$, we have consistency with the existing radio data for all blazars.

We conclude that the available low-frequency radio data do not exclude the presence of extended emission in our blazars, and that CMB quenching is instrumental in reducing the radio-lobe emission below current detection limits in all sky surveys.

Our modelling relies on a number of assumptions on the fiducial values of key parameters, and the resulting SEDs are degenerate with respect to, e.g. the values of the magnetic field strength and of the source size. On the other hand, deeper observations by, e.g. LOFAR, should be able to detect the lobe radio emission in most sources, even in the conservative case $P_{e,lobe} = 0.01\,P_{jet}$. Should the radio (and/or the X-ray) flux of the lobes be detected, the source physical parameters would be determined with much higher confidence. While in principle a simple low-frequency excess of the radio flux above the extrapolation of the flat jet spectrum marks the presence of a lobe, radio maps (and X-ray detections and, possibly, imaging; see Section 4.1 below) would allow us to measure the magnetic field and the injected power, and hence derive the total electron and magnetic energetics with minimum assumptions.

5 DISCUSSION AND CONCLUSIONS

Previous works (e.g. Volonteri et al. 2011) found that the number density of radio galaxies agrees with the expected parent population of blazars at $z \lesssim 3$. At earlier epochs, however, there is a clear, strong deficit of radio galaxies. One of the possible solutions for this puzzle is the $(1+z)^4$ enhancement of the CMB radiation energy density, which quenches the isotropic radio emission of the lobes while boosts their X-ray luminosity.

We have then constructed a sample containing all known blazars at $z > 4$, modelling their jet emission to ultimately assess the broad-band emission of the lobes. While current low-frequency observations of high-z blazars do not show any evidence of isotropically, optically thin synchrotron emission from extended lobes, our results indicate that such observations are simply not deep enough. We can predict that, for a range of plausible parameters, deeper pointings (by, e.g. LOFAR or by the expanded VLA) should be able to detect the lobe emission. At the same time, deep X-ray observations with high angular resolution (by, i.e. *Chandra*) have the required sensitivity to detect and resolve the lobes in X-rays, as the estimated lobe angular size is large enough to avoid flux contamination from the point-like nuclear emission.

A measure of the lobe radio and X-ray fluxes, as well as of the lobe angular size, will allow us to estimate the physical parameters of the source with no ambiguity and without invoking equipartition between the particles and the magnetic field. Besides testing the validity of the CMB quenching scenario, this will give information about the energy in the proton component of the lobes, and possibly the coherence length of the magnetic field.

According to our scenario, if the lobes were indeed large (namely, $R_{lobe} > 25$ kpc) and in equipartition, then it would be difficult to detect them in any radio galaxy in the radio band at high redshifts.

Downloaded from https://academic.oup.com/mnras/article-abstract/452/4/3457/1060612 by INAF Brera Milano (Osservatorio Astronomico di Brera) user on 28 February 2020

Table 3. Adopted parameters for the jet models shown in Fig. 8. Column [1]: name; Column [2]: redshift; Column [3]: distance of the dissipation region from the black hole, in units of 10^{15} cm; Column [4]: size of the BLR, in units of 10^{15} cm; Column [5]: power injected in the jet in relativistic electrons, calculated in the comoving frame, in units of 10^{45} erg s^{-1}; Column [6]: magnetic field in G; Column [7]: bulk Lorentz factor; Column [8]: viewing angle in degrees; Columns [9] and [10]: break and maximum Lorenz factor of the injected electron distribution; Columns [11] and [12]: slopes of the injected electron distribution; Column [13]: logarithm of jet power in the form of radiation, in erg s^{-1}; Column [14]: logarithm of the total kinetic plus magnetic jet power, in erg s^{-1}. The values of the powers and the energetics refer to *one* jet.

Name [1]	z [2]	$R_{\rm diss}$ [3]	$R_{\rm BLR}$ [4]	$P'_{\rm e,jet,45}$ [5]	B [6]	Γ [7]	$\theta_{\rm V}$ [8]	$\gamma_{\rm b}$ [9]	$\gamma_{\rm max}$ [10]	s_1 [11]	s_2 [12]	$\log P_{\rm r}$ [13]	$\log P_{\rm jet}$ [14]
0324−2918	4.630	1200	1140	0.02	2.4	13	3	150	2e3	–1	2.8	46.0	46.9
0525−3343	4.413	630	1643	0.06	2.9	15	3	50	3e3	0	2.4	46.1	47.5
0839+5112	4.390	1470	1336	0.04	1.2	13	4	90	4e3	0	2.6	45.8	47.2
0906+6930	5.47	630	822	0.02	1.8	13	3	100	3e3	0	2.5	46.0	46.8
1026+2542	5.304	504	916	0.01	2.3	13	3	70	4e3	0	2.6	45.7	46.7
1028−0844	4.276	840	1095	0.08	1.4	15	3	100	4e3	0	2.6	46.2	47.4
1146+4037	5.005	900	1006	7e–3	1.4	13	3	130	3e3	0	2.6	45.6	46.4
1253−4059	4.460	480	671	0.02	1.8	13	3	100	3e3	1	2.5	45.5	47.2
1309+5733	4.268	1200	756	3e–3	0.5	12	3	20	3e3	0	2.7	44.6	46.2
1325+1123	4.412	900	739	9e–3	1.9	12	3	250	3e3	0	2.6	45.5	46.3
1420+1205	4.034	360	725	6e–3	2.6	13	3	120	3e3	1	2.5	45.5	46.7
1430+4204	4.715	540	1112	0.1	1.7	14	3	40	3e3	0	2.6	46.8	47.9
1510+5702	4.309	293	636	0.04	2.6	15	3	60	4e3	0.5	2.6	46.4	47.5
1715+2145	4.011	396	233	0.013	0.65	15	3	220	3e3	1.5	3.2	45.3	47.2
2134−0419	4.346	432	972	7e–3	2.9	13	3	70	4e3	0	2.6	45.5	46.6
2220+0025	4.205	360	671	3e–3	2.4	13	3	120	3e3	1	2.2	45.2	46.4

The radio galaxies at $z > 4$ with detected extended radio emission apparently challenge our proposed CMB quenching scenario (see e.g. TN0924–2201 at $z = 5.19$, van Breugel et al. 1999; 6C 0140+326 at $z = 4.41$, Rawlings et al. 1996; 4C 63.20 at $z = 4.261$, Lacy et al. 1994a; PKS 1338−1942 at $z = 4.11$, De Breuck et al. 1999). We defer a detailed study of these sources to a paper in preparation, yet we can anticipate that the reason of their strong radio emission most probably lies in the fact that what we detect are the hotspots, not the lobes (see e.g. De Breuck et al. 2010 for an estimate of the lobe sizes). The strong magnetic field of their hotspots (of the order of hundreds of μG), makes synchrotron losses competitive with the inverse Compton scattering off CMB photons.

Our results have a profound impact on the estimated fraction of radio-loud high-z AGNs. The jet emission in blazars is in fact easily visible even at high redshifts and is unaffected by the CMB quenching since: (i) jet emission is strongly enhanced by beaming, and (ii) the radio flux originates in compact regions where magnetic energy density dominates over the CMB. The beaming pattern of jet emission decreases fast for increasing viewing angles: for $\Gamma = 15$, the flux at $\theta_{\rm v} \sim 15^\circ$ is dimmed by ∼5 orders of magnitude compared to the one at $\theta_{\rm v} = 3^\circ$. This implies that misaligned, high-z jets are invisible for the sensitivity of current instruments.

Fig. 9 illustrates the point. We compare the SED of 1026+2542 ($z = 5.3$) computed in Section 4 to the corresponding model as observed at viewing angle $\theta_{\rm v} = 15^\circ$. By modelling the hotspot + lobe emission as detailed in Section 3.3 (green line in Fig. 9), we find that the resulting isotropic radio flux would reach the mJy level at frequencies ≃300 MHz, and would be much weaker at higher frequencies. As a result, a source like 1026+2542 whose jet is observed at $\theta_{\rm v} > 15^\circ$ would be easily detected in current optical survey, thanks to its quasi-isotropic accretion disc emission, but would fail to enter radio catalogues like FIRST, with its sensitivity limit of 1 mJy at 1.4 GHz. *Therefore, slightly misaligned high-z jetted sources would be classified as radio quiet*. The very term 'radio loud' becomes misleading. The idea that some high-z radio-quiet AGNs could have extended X-ray emission, revealing the presence of the jet, was first put forward by Schwartz (2002) analysing the X-ray data of three $z \sim 6$ radio-quiet sources observed by *Chandra*. The short exposure of these observations seemed to suggest that the X-ray emission was *extended*. However, the extended emission of one of them was then associated to a galaxy (Ivanov 2002), and this was confirmed by longer *Chandra* observations by Schwartz & Virani (2004). Brandt et al. (2002) did not confirm the extended nature of the X-ray flux observed in the other two sources.

Fig. 9 also shows that most of the lobe radiative losses are instead in the X-ray band. Electrons emitting above ≃1 keV are cooling in less than one source crossing time, and therefore are responsible for releasing almost the entire injected power $P_{\rm e}^{\rm lobe} \sim 0.1\, P_{\rm jet} = 5 \times 10^{45}$ erg s^{-1}. Lobes are then radio-quiet and X-ray loud. Interestingly, in the 2–10 keV X-ray band the extended lobe and the nuclear accretion disc corona emissions can be comparable, as shown in Fig. 9. As a linear proper dimension of 100 kpc corresponds at $z = 5$ to an angular size of 16 arcsec, sub-arcmin X-ray imaging is required to disentangle the two components.

Downloaded from https://academic.oup.com/mnras/article-abstract/452/4/3457/1060612 by INAF Brera Milano (Osservatorio Astronomico di Brera) user on 28 February 2020

Table 4. Adopted parameters for the hotspot and lobe models shown in Figs 7 and 8. For each source, the first raw corresponds to $P_e/P_{jet} = 0.1$, while the second raw corresponds to $P_e/P_{jet} = 10^{-2}$. Column [1]: name; Column [2]: logarithm of the power injected throughout the hotspots and lobes in relativistic electrons in erg s^{-1}; Column [3]: magnetic field of the hotspot in μG; Column [4]: logarithm of the energy in magnetic field contained in the hotspot, in erg; Column [5]: magnetic field of the lobe in μG; Column [6]: logarithm of the energy in magnetic field contained in the lobe, in erg; All sources have $R_{HS} = 2$ kpc, $R_{lobe} = 50$ kpc, $\gamma_b = 10^3$, $\gamma_{max} = 10^6$ and slopes of the injected electron distribution $s_1 = -1$ and $s_2 = 2.7$. The values of the powers and the energetics refer to *one* jet and *one* hotspot and lobe, while the lobe flux shown in the figures corresponds to *two* hotspots and lobes. *: for this source the hotspot is detected, so we have used the observed $R_{HS} = 1.5$ kpc. The magnetic field is found without invoking equipartition, and the electron energy of the hotspot is $\log(E_{e,HS}/\mathrm{erg}) = 57.1$.

Name [1]	log P_e [2]	B_{HS} [3]	log $E_{B,HS}$ [4]	B_{lobe} [5]	log $E_{B,lobe}$ [6]
0324−2918	45.9	172	57.1	13.5	59.1
	44.9	52.2	56.0	13.5	58.1
0525−3343	46.5	319	57.6	26	59.6
	45.5	105	56.7	8.2	58.6
0839+5112	46.2	233	57.3	18.2	59.3
	45.2	71	56.3	5.8	58.3
0906+6930	45.8	151	56.9	11.9	59.9
	44.8	47	55.9	3.77	57.9
1026+2542	45.7	130	56.8	10.5	58.8
	44.7	41.2	55.8	3.32	57.8
1028−0844	46.4	310	57.6	24.5	59.6
	45.4	97	56.6	7.8	58.6
1146+4037	45.4	95	56.6	7.53	58.5
	44.4	29.3	55.5	2.4	57.5
1253−4059	46.2	233	57.3	18.1	59.3
	45.2	71.4	56.3	5.8	58.3
1309+5733	45.0	56.8	56.1	4.8	58.2
	44.0	16.5	55.0	1.51	57.1
1325+1123	45.3	82	56.5	6.7	58.4
	44.3	24.2	55.4	2.12	57.4
1420+1205	45.7	138	56.9	11.1	58.9
	44.7	39	55.8	3.3	57.8
1430+4204	46.9	510	58.0	41	60.0
	45.9	169	57.0	13.2	59.0
1510+5702	46.5	335	57.6	26.8	59.6
	45.5	106	56.6	8.5	58.6
1715+2145*	46.1	190	56.8	20.3	59.4
2134−0419	45.6	115	56.7	9.35	58.7
	44.5	34.3	55.7	2.95	57.7
2220+0025	45.4	89	56.5	7.23	58.5
	44.4	25.5	55.4	2.3	57.5

ACKNOWLEDGEMENTS

We thank the referee, John Wardle, for very useful comments and criticisms, that helped to improve the paper. This research made use of the NASA/IPAC Extragalactic Database (NED) which is operated by the Jet Propulsion Laboratory, Caltech, under contract with NASA. Part of this work is based on archival data, software or online services provided by the ASI Science Data Center (ASDC).

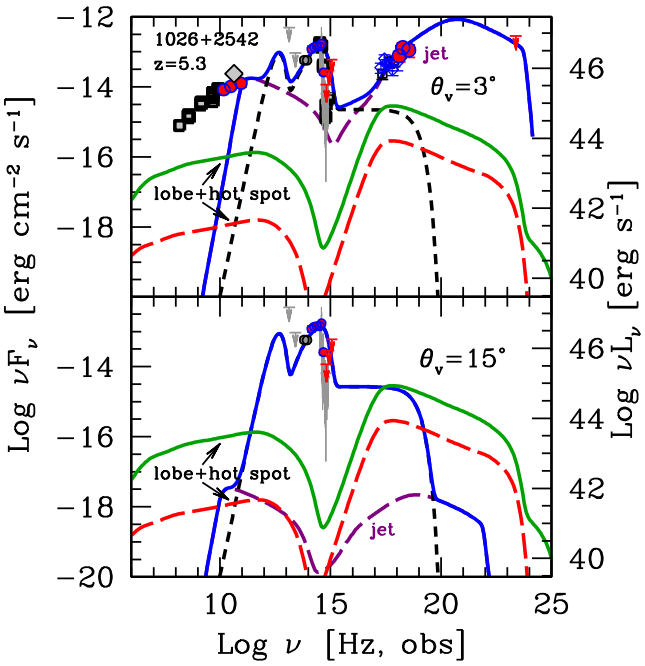


Figure 9. Top panel: the SED of the blazar 1026+2542 at $z = 5.3$ is fitted with a model (parameters in Table 3) with $\Gamma = 15$ and $\theta_v = 3°$, as in Fig. 8. Here we also show the contribution from the jet (long-dashed violet line), the thermal components (disc, torus and corona, as a short-dashed black line) and their sum (solid blue line). The solid green and the dot–dashed red lines are the estimated lobe + hotspot emission as in Fig. 8 (the two models differ from the assumed injected electron energy, equal to 10 per cent of 1 per cent of P_{jet}, respectively). Bottom panel: if the very same source is observed at $\theta_v = 15°$ (i.e. only slightly off the beaming angle), the jet emission (long-dashed red line) is so weak that it would be missed by all current surveys, while the isotropic components (disc, torus, corona and the lobes) would remain the same. *Current optical surveys, as the SDSS, would easily detect the source, and classify it as a radio-quiet quasar.* The lobe + hotspot emission, slightly below the sensitivity of FIRST (1 mJy at 1.4 GHz), could be detectable by LOFAR (see Fig. 8); furthermore, pointed *Chandra* X-ray observations could detect and resolve the X-ray emission of the lobes (note that 50 kpc at $z = 5.3$ correspond to an angular size of 8.2 arcsec in the adopted cosmology). These observations could establish the jetted nature of the source.

REFERENCES

Ackermann M. et al., 2011, ApJ, 743, 171
Ajello M. et al., 2009, ApJ, 699, 603
Bassett L. C., Brandt W. N., Schneider D. P., Vignali C., Chartas G., Garmire G. P., 2004, AJ, 128, 523
Belsole E., Worrall D. M., Hardcastle M. J., Birkinshaw M., Lawrence C. R., 2004, MNRAS, 352, 924
Brandt W. N. et al., 2002, ApJ, 569, L5
Carilli C. L., Taylor G. B., 2002, ARA&A, 40, 319
Celotti A., Fabian A. C., 2004, MNRAS, 353, 523
Croston J. H., Birkinshaw M., Hardcastle M. J., Worrall D. M., 2004, MNRAS, 353, 879
Croston J. H., Hardcastle M. J., Harris D. E., Belsole E., Birkinshaw M., Worrall D. M., 2005, ApJ, 626, 733
De Breuck C., van Breugel W., Minniti D., Miley G., Röttgering H., Stanford S. A., Carilli C., 1999, A&A, 352, L51
De Breuck C. et al., 2010, ApJ, 725, 36
de Vries W. H., Becker R. H., White R. L., 2006, AJ, 131, 666
Fabian A. C., Celotti A., Iwasawa K., Ghisellini G., 2001b, MNRAS, 324, 628

Downloaded from https://academic.oup.com/mnras/article-abstract/452/4/3457/1060612 by INAF Brera Milano (Osservatorio Astronomico di Brera) user on 28 February 2020

Fabian A. C., Celotti A., Iwasawa K., McMahon R. G., Carilli C. L., Brandt W. N., Ghisellini G., Hook I. M., 2001a, MNRAS, 323, 373
Ghisellini G., 1999, Astron. Nachr., 320, 232
Ghisellini G., Tavecchio F., 2009, MNRAS, 397, 985
Ghisellini G., Tavecchio F., 2010, MNRAS, 409, L79
Ghisellini G., Tavecchio F., 2015, MNRAS, 448, 1060
Ghisellini G., Celotti A., Tavecchio F., Haardt F., Sbarrato T., 2014a, MNRAS, 438, 2694
Ghisellini G., Sbarrato T., Tagliaferri G., Foschini L., Tavecchio F., Ghirlanda G., Braito V., Gehrels N., 2014b, MNRAS, 440, L111
Ghisellini G., Tavecchio F., Maraschi L., Celotti A., Sbarrato T., 2014c, Nature, 515, 376
Ghisellini G., Tagliaferri G., Sbarrato T., Gehrels N., 2015, MNRAS, 450, L34
Gobeille D. B., Wardle J. F. C., Cheung C. C., 2014, preprint (arXiv: 1406.4797)
Haiman Z., Quataert E., Bower G. C., 2004, ApJ, 612, 698
Hardcastle M. J., Krause M. G. H., 2014, MNRAS, 443, 1482
Hook I. M., McMahon R. G., 1998, MNRAS, 294, L7
Hook I. M., McMahon R. G., Shaver P. A., Snellen I. A. G., 2002, A&A, 391, 509
Ivanov V. D., 2002, A&A, 389, L37
Kratzer R. M., Richards G. T., 2015, AJ, 149, 61
Lacy M. et al., 1994, MNRAS, 271, 504
Mc Greer I. D., Helfand D. J., White R. L., 2009, AJ, 138, 1925
Massaro F., Giroletti M., Paggi A., D'Abrusco R., Tosti G., Funk S., 2013, ApJS, 208, 15
Mocz P., Fabian A. C., Blundell K. M., 2011, MNRAS, 413, 1107
Nemmen R. S., Georganopoulos M., Guiriec S., Meyer E. T., Gehrels N., Sambruna R. M., 2012, Science, 338, 1445
Rawlings S., Lacy M., Blundell K. M., Eales S. A., Bunker A. J., Garrington S. T., 1996, Nature, 383, 502
Rees M. J., 1978, MNRAS, 184, P61
Romani R. W., Sowards-Emmerd D., Greenhill L., Michelson P., 2004, ApJ, 610, L9
Sbarrato T. et al., 2012, MNRAS, 426, L91
Sbarrato T., Ghisellini G., Nardini M., Tagliaferri G., Greiner J., Rau A., Schady P., 2013a, MNRAS, 433, 2182
Sbarrato T. et al., 2013b, ApJ, 777, 147
Sbarrato T., Ghisellini G., Tagliaferri G., Foschini L., Nardini M., Tavecchio F., Gehrels N., 2015, MNRAS, 446, 2483
Schoenmakers A. P., Mack K.-H., de Bruyn A. G., Röttgering H. J. A., Klein U., van der Laan H., 2000, A&AS, 146, 293
Schwartz D. A., 2002, ApJ, 571, L71
Schwartz D. A., Virani S. N., 2004, ApJ, 615, L21
Shakura N. I., Sunyaev R. A., 1973, A&A, 24, 337
Shaw M. S. et al., 2012, ApJ, 748, 49
Shen Y. et al., 2011, ApJS, 194, 45 (S11)
Spada M., Ghisellini G., Lazzati D., Celotti A., 2001, MNRAS, 325, 1559
van Breugel W., De Breuck C. Stanford S. A., Stern D., Röttgering H., Miley G., 1999, ApJ, 518, L61
van Haarlem M. P. et al., 2013, A&A, 556, 2
Van Velzen S., Falcke H., Körding E., 2015, MNRAS, 446, 2985
Volonteri M., Haardt F., Ghisellini G., Della Ceca R., 2011, MNRAS, 416, 216
Wilson A. S., Yoing A. J., Shopbell P. L., 2000, ApJ, 544, L27
Wu J., Brandt W. N., Miller B. P., Garmire G. P., Schneider D. P., Vignali C., 2013, ApJ, 763, 109
Yuan W., Matsuoka M., Wang T., Ueno S., Kubo H., Mihara T., 2000, ApJ, 545, 625
Yuan W., Fabian A. C., Worsley M. A., McMahon R. G., 2006, MNRAS, 368, 985

This paper has been typeset from a TEX/LATEX file prepared by the author.

Downloaded from https://academic.oup.com/mnras/article-abstract/452/4/3457/1060612 by INAF Brera Milano (Osservatorio Astronomico di Brera) user on 28 February 2020